

Full paper

Coupling of piezoelectric, semiconducting and photoexcitation properties in NaNbO_3 nanostructures for controlling electrical transport: Realizing an efficient piezo-photoanode and piezo-photocatalyst



Simrjit Singh, Neeraj Khare*

Department of Physics, Indian Institute of Technology Delhi, Hauz Khas, New Delhi 110016, India

ARTICLE INFO

Keywords:

Ferroelectric
Piezophototronic
 NaNbO_3
Photoelectrochemical
Photocatalytic

ABSTRACT

Piezophototronic effect in semiconductors such as ZnO and BaTiO_3 has been studied earlier but chemical instability and **insulating** nature of these respective materials make them unsuitable for photoelectrochemical (PEC) and photocatalytic applications. Herein, we demonstrate an efficient coupling between piezoelectric, semiconducting and photoexcitation properties in chemically stable NaNbO_3 semiconductor with an aim to enhance the efficiency of PEC water splitting and photocatalytic activities. We show that an alternating **built-in potential** can be generated in NaNbO_3 nanostructures under periodic mechanical strain resulting in improved charge separation of the photogenerated charge carriers. NaNbO_3 particulate suspension shows a large (~115%) enhancement in the photodegradation rate of organic dyes in industrial waste water which is much higher than the earlier reported piezophotocatalytic activity in ZnO. For PEC water splitting activity, NaNbO_3 nanostructure films deposited onto flexible ITO coated **polyethylene terephthalate** (ITO/PET) substrates were polarized by applying an external electric field. Enhancement in the **photocurrent** density from 0.78 mA/cm^2 to 1.02 mA/cm^2 and ~8% improvement in the **incident photon to current conversion efficiency** have been noted under the piezoassistance. Our present work demonstrates an efficient coupling between mechanical, optical and electrical properties in NaNbO_3 thus, it can be used as a potential alternative material for piezophototronic applications.

1. Introduction

The discovery of **piezophototronic effect** by Wang et al. has inspired worldwide attention in fabricating new electronic and optoelectronic devices [1–4]. In the piezophototronic effect, the generation of piezopotential under mechanical strain strongly affects the charge transport properties of piezoelectric-semiconductors. An improved performance of the devices such as photodetectors, solar cells and light emitting **diodes** has already been demonstrated using this effect [5–10]. However, comparatively very less attention has been paid in utilizing this effect for electrochemical and catalytic applications [11,12]. Photoelectrochemical (PEC) water splitting and photocatalytic (PC) degradation of organic dyes are among the promising solutions for global energy and environmental crisis, respectively [13,14]. Thus, more attention should be given in enhancing the activities of these two valuable processes using the piezophototronic effect. For studying this effect, semiconductor nanostructures with one dimensional (1D) geometry are ideal as these can bear an ample mechanical strain. Currently, ZnO is the most preferred and widely used material for studying piezophototronic effect which is possibly due to its low cost

synthesis, environment friendly nature and good semiconducting characteristics [11,15]. Shi et al. [16] demonstrated **tuning** of photoelectrochemical water splitting activity using ZnO semiconductor by controlling the **barrier height** by piezoelectric polarization. Recently, Xue et al. [17] showed piezopotential endowed enhancement in the photocatalytic activity using ZnO nanowires. An indirect approach by combining piezoelectric BaTiO_3 with other **photoactive** semiconductor such as Ag_2O is also demonstrated by Li et al. [12] in which an enhancement in the charge transport property of semiconductor is obtained by using the piezoelectric effect of BaTiO_3 . **However, most widely studied ZnO due to its chemical instability in alkaline as well as acidic media and BaTiO_3 due to its insulating characteristics are not very suitable materials for practical applications** [18]. Thus, there is a need to look for other piezoelectric-semiconductor materials for specifically studying PEC and PC activities.

In the quest for a single phase compound possessing both piezoelectric as well as semiconducting properties, NaNbO_3 can be an optimum choice of material which exhibit **n-type conductivity** and ferroelectric characteristics at room temperature [19,20]. It also possesses an excellent chemical stability and high mobility of charge

* Corresponding author.

E-mail address: nkhare@physics.iitd.ernet.ac.in (N. Khare).

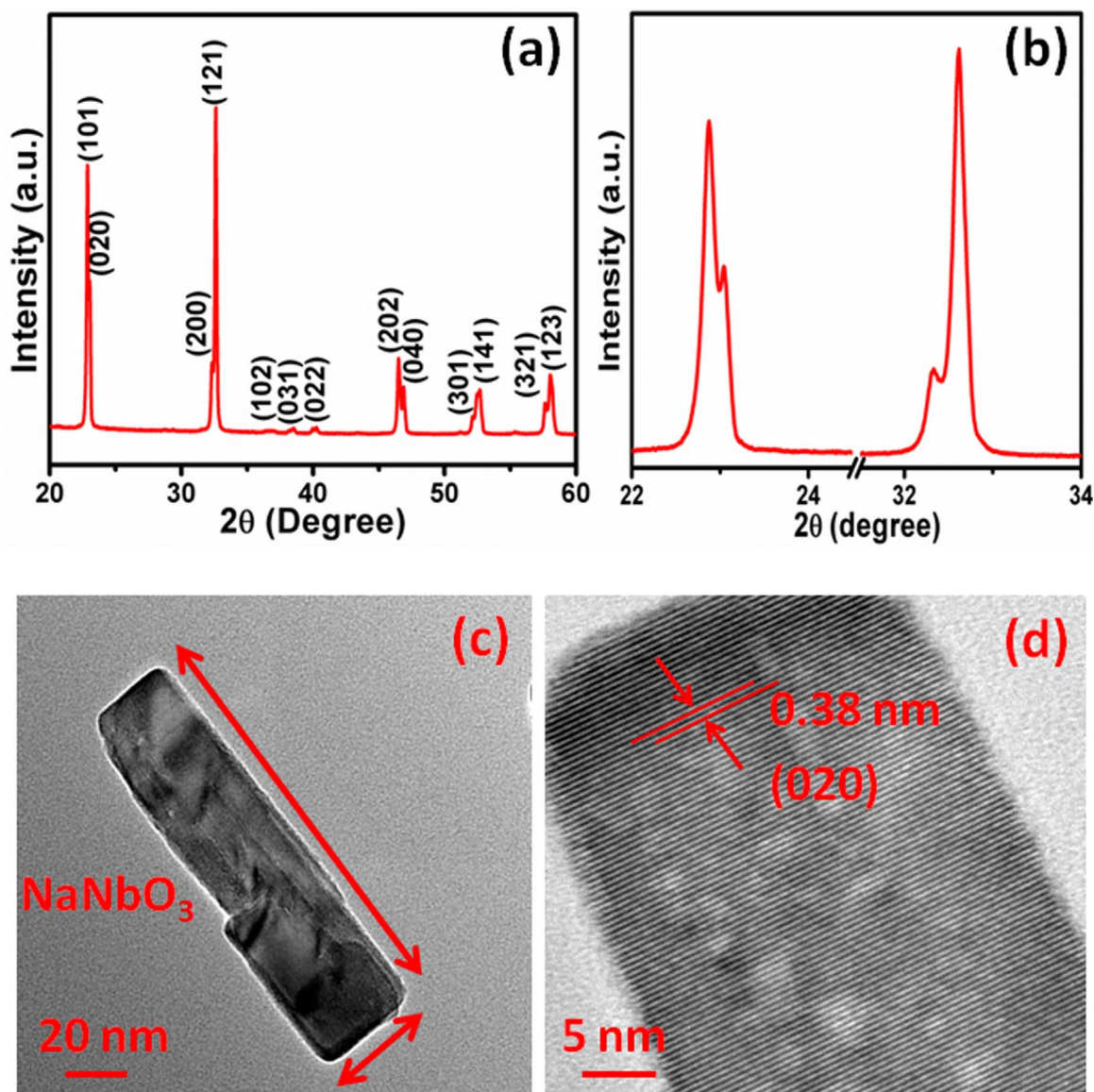


Fig. 1. Structural analysis of NaNbO₃ nanostructures. (a, b) XRD patterns of NaNbO₃ nanorods; (c, d) TEM and HRTEM image of NaNbO₃ nanorods.

carriers [21]. To the best of our knowledge, the potential of NaNbO₃ nanostructures for PC and PEC applications by utilizing the piezotronic effect has not been studied earlier.

The aim of the present study is to demonstrate piezopotential enhanced enhancement in the photoanodic activity of NaNbO₃ nanostructure films for PEC water splitting and enhancement in the photocatalytic activity of NaNbO₃ particulate suspension for degradation of methylene blue organic dye. We show much improved performance of NaNbO₃ nanostructures in the photocatalytic degradation of organic dye compared to previously reported ZnO nanostructures under the piezophototronic effect.

2. Results and discussions

X-ray diffraction patterns (Fig. 1a and b) and X-ray photoelectron spectra (See Supporting information, Fig. S1) confirms the single phase formation of NaNbO₃ nanostructures. Doublets in the XRD peaks indicate the formation of orthorhombic crystal structure. Further, the rietveld refinement of XRD data (See Supporting information, Fig. S2) gives lattice parameters of $a=5.565$ Å, $b=7.776$ Å and $c=5.514$ Å with P2₁ma ferroelectric symmetry. The P2₁ma ferroelectric symmetry of NaNbO₃ is very crucial for studying piezophototronic effect as it

exhibits large piezoelectricity. Fig. 1c and d show transmission electron microscopy (TEM) and high resolution TEM images respectively, which reveal rod like structure of NaNbO₃. The length and diameter of the nanorod is ~150 nm and ~40 nm respectively. The HRTEM image of nanorod exhibits clear lattice fringes with d-spacing ~3.8 Å corresponding to (020) plane which further suggest good crystalline quality of the nanorods.

The optical bandgap of NaNbO₃ nanostructure film coated onto quartz substrate has been determined using the Tauc's relation (Fig. 2a) [22]. By extrapolating the linear portion of a plot between $(\alpha h\nu)^2$ vs. $(h\nu)$ to zero, a bandgap value of ~3.36 eV is obtained. This value is comparable to the values of bandgap of NaNbO₃ reported in the literature [21,23–25]. For the determination of conduction band (CB) and valence band (VB) positions of NaNbO₃, the valence band spectrum has also been recorded using the XPS measurement (Fig. 2b). A valence band position at ~2.56 eV is obtained from the XPS analysis. From energy bandgap value and VB position, the CB position is obtained at ~-0.8 eV. The estimated CB and VB positions are energetically favorable to carry out oxidation and reduction reactions for the generation of oxygen and hydrogen, respectively in the PEC process [26]. In addition, the estimated CB position of NaNbO₃ is ~300 meV more negative than the CB position of ZnO which make it

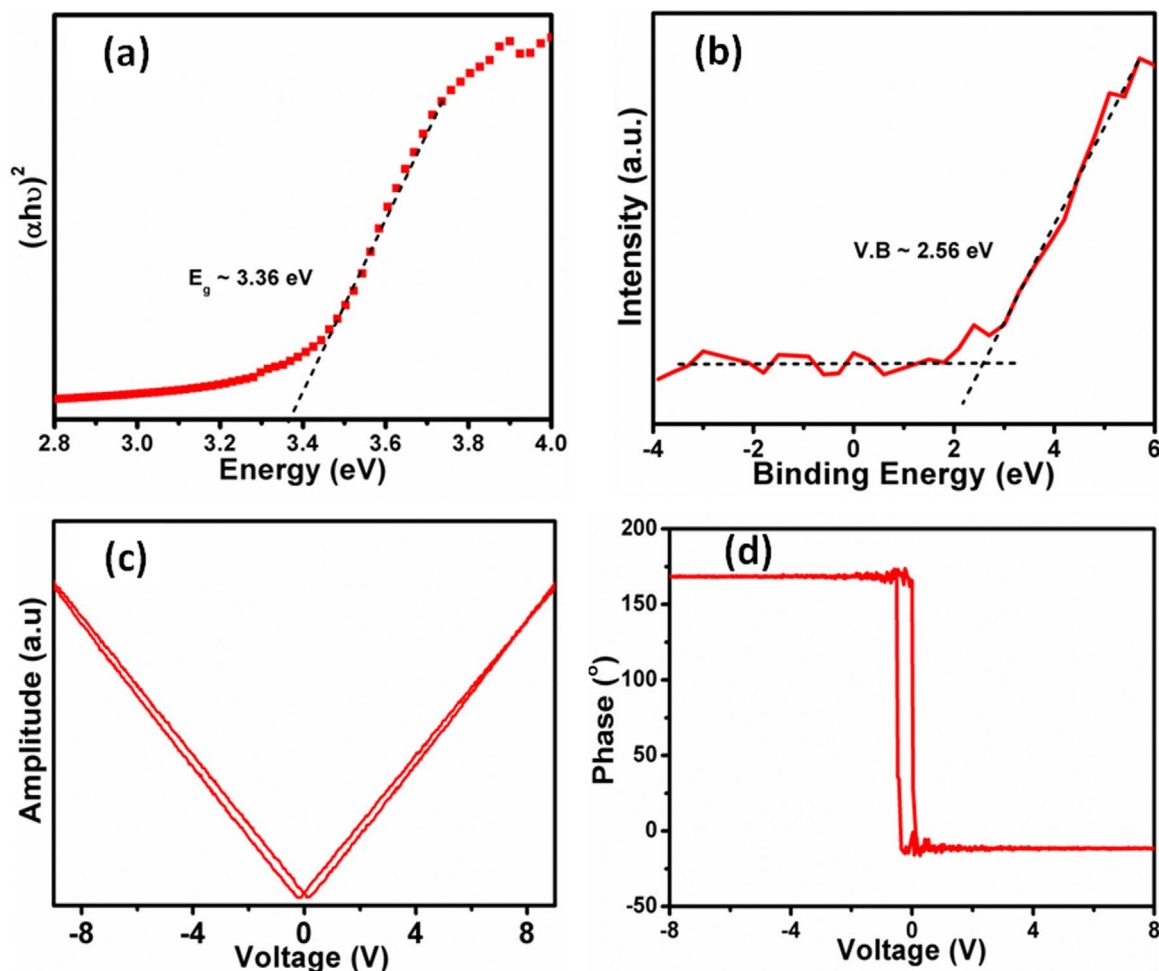


Fig. 2. (a) Optical bandgap of NaNbO₃ nanostructure film, (b) Valence band spectrum of NaNbO₃ nanostructure film, (c) PFM amplitude butterfly loop and (d) PFM phase hysteresis loop of NaNbO₃ nanostructure films coated onto ITO/PET substrate.

more energetically favorable for photo assisted water splitting [27].

To probe piezo/ferroelectric properties in NaNbO₃ nanostructures, piezoresponse force microscopy (PFM) technique has been employed. A localized point to point piezo-response of the nanostructure film coated onto flexible ITO coated polyethylene terephthalate (ITO/PET) substrate has been probed by applying a probe bias of ± 8 V. Fig. 2c and d represent PFM amplitude and phase signals, respectively. The amplitude signal (Fig. 2c) shows polarization amplitude whereas, phase signal (Fig. 2d) measures the polarization direction. The sample shows well defined phase hysteresis and amplitude butterfly loop which reveal non-zero remnant polarization or ferroelectric character exhibited by the film. However, a small phase hysteresis (indicated from smaller loop area) exhibited by the film represents weak ferroelectric character which can be due to semiconducting nature of NaNbO₃. Further, we also determined piezoelectric coefficient (d_{33}) from the PFM amplitude data to quantify the net polarization in our NaNbO₃ sample. A d_{33} value of ~ 52.5 pm/V is obtained. The observed d_{33} value for NaNbO₃ is higher than the d_{33} value reported for ZnO nanostructures [28,29].

For studying potential of piezophototronic effect for the catalytic degradation of organic dye, the degradation capability of methylene blue (MB) dye has been evaluated in dark and UV light under two different conditions i.e. physical mixing and ultrasonic vibrations (Fig. 3). The ultrasonic vibrations will result in an alternating built-in electric field which will separate the photogenerated charge carriers incessantly and can result in the enhancement of the photocatalytic activity for longer durations. From Fig. 3a it can be clearly seen that negligible degradation of MB is observed when the catalytic experiment is performed under dark with physical mixing. However, when reaction

system is subjected to ultrasonic vibrations, a relatively small increase in the degradation activity is observed (Fig. 3b). To see the photo effect, the catalytic experiment has been performed under UV light irradiations (intensity ~ 100 mW/cm²) with physical mixing. A significant photocatalytic activity of NaNbO₃ nanostructures is observed for the degradation of MB dye (Fig. 3c). Under the combined effect of UV light and ultrasonic vibrations, the degradation rate of MB dye is enhanced compared to photocatalytic activity under physical mixing (Fig. 3d). Fig. 3e shows the normalized concentration plots which are obtained by integrating the area of absorption peaks at different intervals of time. The corresponding rate constants have been determined by fitting the experimental data points into pseudo first order kinetic equation [30]; $\ln \frac{C_0}{C} = kt$ and are shown in Fig. 3f. The normalized concentration and rate constant plots clearly reveals enhancement in the degradation rate under ultrasonic vibrations. A large $\sim 115\%$ enhancement in the photodegradation rate using NaNbO₃ is observed when catalytic experiment was performed under ultrasonic vibrations as compared to when performed under physical mixing condition. This enhancement in the photocatalytic activity is correlated to the piezophototronic effect. In piezoelectric materials, the periodic ultrasonic vibrations can generate mechanical strain which can induce a piezoelectric potential. The generation of piezo-potential in NaNbO₃ led to an effective separation of photogenerated electrons/holes and these electrons/holes migrate to the surface of NaNbO₃ where they react with adsorbed oxygen (O₂) and hydroxide ions (OH⁻) to form superoxide anion (O₂⁻) radicals and hydroxyl (OH[·]) radicals. Finally, these free radicals oxidize the MB organic dye in the aqueous solution.

The observed increase in the photodegradation efficiency under

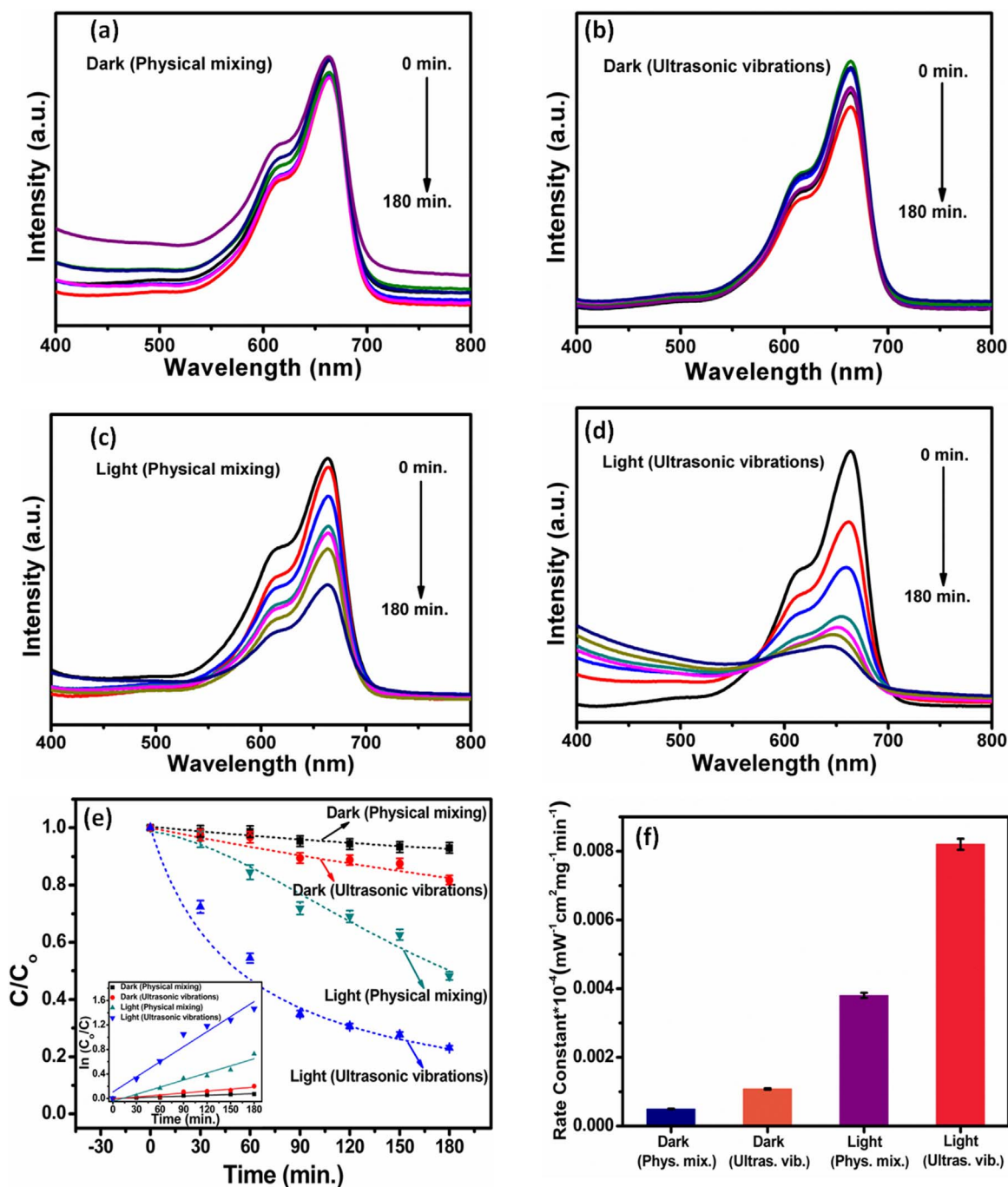


Fig. 3. Photocatalytic degradation activity of NaNbO_3 particulate suspension (a) under dark with physical mixing, (b) under dark with ultrasonic vibrations, (c) under light with physical mixing, (d) under light with ultrasonic vibrations, (e) comparison of the photocatalytic degradation efficiency performed under different experimental conditions (dotted lines connecting to the dots are guide to the eye only) Inset of Fig. (e) shows kinetics fit to the data, (f) comparison of the rate constant values for the degradation of MB dye.

piezo-assistance is also found to be very much higher as compared to earlier reported piezoassisted catalytic activity (i.e. 32%) using ZnO nanowires [17]. In spite of the higher resistance of NaNbO_3 as compared to ZnO (The I-V characteristic of NaNbO_3 nanostructure film is shown in Fig. S3 of Supporting information), this enhancement can be due to higher piezoelectric coefficient possessed by NaNbO_3 nanostructures (~ 52.5 pm/V) as compared to ZnO nanostructures [28,29]. Due to larger value, during the application of periodic ultrasonic vibrations, a higher alternating built-in electric field can be generated inside the NaNbO_3 nanorods which help in the effective separation of the photogenerated charge carriers leading to enhanced degradation of methylene blue organic dye.

Fig. 4 describes the schematic representation of the working

mechanism of piezoelectric NaNbO_3 nanorods for the enhanced degradation rate of MB organic dye under the effect of periodic mechanical vibrations. The exposure of NaNbO_3 to the UV light leads to the generation of photoelectrons and photoholes which participate in the chemical reactions at the surface of NaNbO_3 and generate hydroxyl (OH) and superoxide anion (O_2^-) radicals. These hydroxyl and superoxide anion radicals participate in the degradation of MB organic dye. As the value of piezoelectric coefficient (d_{33}) for NaNbO_3 is large (~ 52.5 pm/V), a significant polarization will result when it is exposed to ultrasonic vibrations. Under the effect of piezo-potential, the recombination rate of photogenerated electron-hole pairs is greatly reduced thus, more charge carriers can migrate to the surface of NaNbO_3 which enhances the formation of OH and O_2^- radicals. The

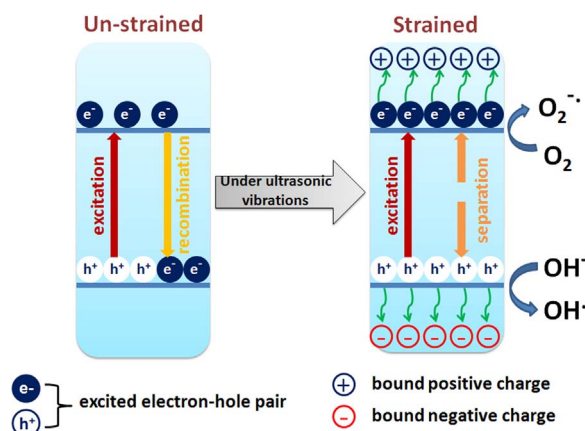
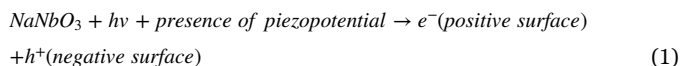


Fig. 4. Schematic diagrams showing the mechanism of the photogenerated charge carriers separation in the un-strained and strained NaNbO₃ nanorods.

availability of more free radicals under the effect of piezopotential enhances the degradation rate of MB organic dye. The reaction mechanism for the piezophotocatalytic activity can be described as follows [31];



Further, we also demonstrate potential of piezoelectric NaNbO₃ nanostructures for enhancing the photoelectrochemical water splitting activity. For PEC activity, spray coated films of NaNbO₃ nanostructures on flexible ITO/PET substrates were used. Prior to measurements, the films were polarized (to align the randomly oriented dipoles) by applying an external bias of 8 V to the films. The bias is applied in such a manner so that the bands are bent upward which favors the water oxidation reaction [32]. An experimental setup used for measuring piezophotocatalytic activity is shown in Fig. S4 of Supporting information. Fig. 5 show the results of PEC measurements. Fig. 5a describes the schematic of three electrode assembly used for the PEC measurements which also shows the oxygen (O₂) and hydrogen (H₂) evolution reactions at the respective electrodes. Fig. 5b represents the current vs. potential (J-V) characteristics of NaNbO₃ films under dark, dark with ultrasonic vibrations, under light and light with ultrasonic vibrations conditions. It is evident that the current density is enhanced in dark as well as in light conditions when experiment was performed under ultrasonic vibrations which can be due to the effect of piezopotential on the charge transport properties of NaNbO₃. Compared to the as prepared NaNbO₃ photoanode, photocurrent density is found to enhance from 0.78 mA/cm² to 1.02 mA/cm² under ultrasonic vibrations. A small change in the onset potential of photocurrent under mechanical strain is also observed which indicates the possibility of change in the band alignment at the NaNbO₃/electrolyte interface. In earlier published reports as well, the change in the band alignment has been accounted for the enhancement in the current densities [11,16]. However, in our case the observed change in the onset potential is very small which can be due to periodic nature of mechanical strain (i.e. periodic increase and release of strain). Thus, we may conclude that although change in the band alignment participates, but piezo-potential assisted charge separation phenomenon seems to have dominant role for the observed enhancement in the current density. The charge transfer phenomenon at the interface is further

probed using the electrochemical impedance spectroscopy (EIS) measurements. Fig. 5c shows the EIS Nyquist plots of NaNbO₃ photoanodes. The obtained semi-arcs are simulated using Z-view software to estimate the charge transfer resistance (R_{ct}) at the NaNbO₃/electrolyte interface. The R_{ct} values are found as 1010 Ω, 870 Ω, 810 Ω and 720 Ω when experiments have been performed under dark (without vibrations), dark (with vibrations), light (without vibrations) and light (with vibrations) respectively. The results clearly show a decrease in the charge transfer resistance under ultrasonic vibrations. A decrease in the charge transfer resistance at NaNbO₃/electrolyte interface indicates that more charge carriers can be transferred at the interface for water oxidation reaction [33,34]. Fig. 5d show incident photon to current efficiencies (IPCE) of NaNbO₃ photoanodes under the same experimental conditions. It can be seen that NaNbO₃ possess higher IPCE value when subjected to ultrasonic vibrations. An 8% enhancement in the IPCE is observed when performed under ultrasonic vibrations compared to when performed without ultrasonic vibrations.

Fig. 6 shows schematic representations of the mechanism for the enhanced PEC water splitting activity under ultrasonic vibrations. Fig. 6a describes band edge alignment of n-type NaNbO₃ semiconductor in contact with an electrolyte. At the interface, the energy bands of the semiconductor are bent upward during the equilibrium process of aligning the Fermi level and redox potential of NaNbO₃ and electrolyte respectively. When photons of energy greater than the bandgap of NaNbO₃ semiconductor shine, the electron-hole pairs are generated. The inclination of bands drifts the surface excited electrons towards the semiconductor side and simultaneously holes toward the electrolyte. These holes have sufficient energy (i.e. higher than the oxidation potential) so that these can trigger the oxidation reaction leading to oxygen evolution.

In the presence of ultrasonic vibrations, a piezo-potential is generated in the nanorods in such a way that they attract the photogenerated holes toward the surface at the interface with the electrolyte and also the valence band is lifted more upward so that it become close to the oxidation potential (Fig. 6b). Thus, it becomes more energetically favorable for the holes to participate for the oxidation reaction. At the same time, lifting up of the conduction band at the electrolyte interface accelerates the drift of electrons towards the ITO which finally participate in the hydrogen evolution reaction at the platinum (Pt) counter electrode.

3. Conclusions

To conclude, we demonstrate potential of piezoelectric-NaNbO₃ nanostructures for enhancing the photocatalytic and photoelectrochemical water splitting activity using the piezophotonic effect. NaNbO₃ particulate suspension shows a large (~115%) enhancement in the photocatalytic degradation rate of methylene blue organic dye. During PEC water splitting activity, photocurrent enhancement from ~0.78 mA/cm² to 1.02 mA/cm² and ~8% improvement in the incident photon to current conversion efficiency have been demonstrated under the piezo-assistance. This enhancement is correlated to the piezo-potential induced enhanced separation of the photogenerated charge carriers and band alignment at the NaNbO₃/electrolyte interface.

4. Experimental section

4.1. Synthesis of nanorods

Hydrothermal method was used to prepare NaNbO₃ nanorods. High purity Nb₂O₅ (99.99%) (Sigma Aldrich) and NaOH (99.99%) (Merck) were used as starting materials. For the synthesis, 0.615 g of Nb₂O₅ was dispersed in 80 ml of deionized (DI) water followed by the addition of 9.6 g of NaOH to the above mixture. The mixture was stirred for 2 h at room temperature to mix both the precursors uniformly. Finally, the mixture was transferred to a 100 ml Teflon-

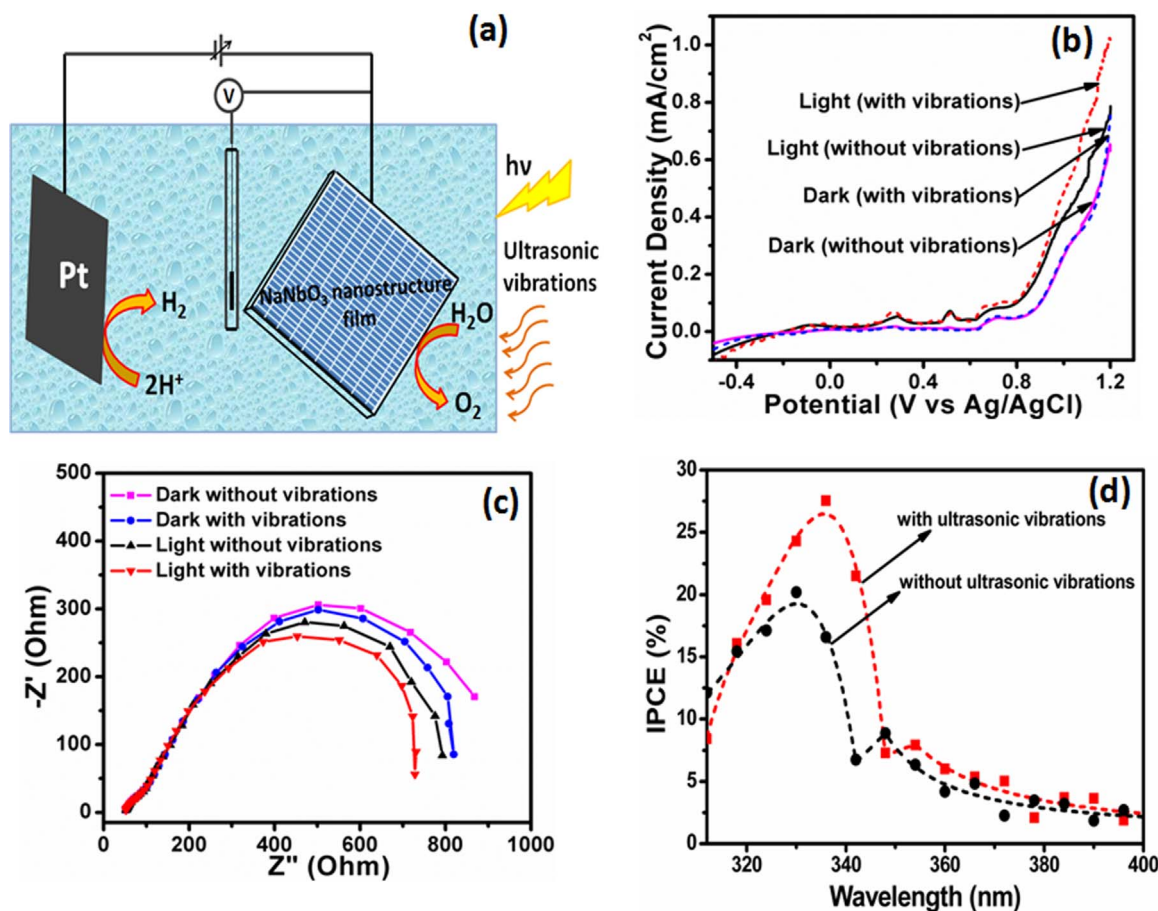


Fig. 5. Photoelectrochemical measurements of NaNbO_3 photoanode (a) PEC three electrode assembly showing overall water splitting reaction mechanism, (b) Current-potential curves of the photoanodes, (c) Electrochemical impedance spectra of the photoanodes under different experimental conditions, (d) Incident photon to current conversion efficiency of the photoanodes (dotted lines connecting to the dots are guide to the eye only).

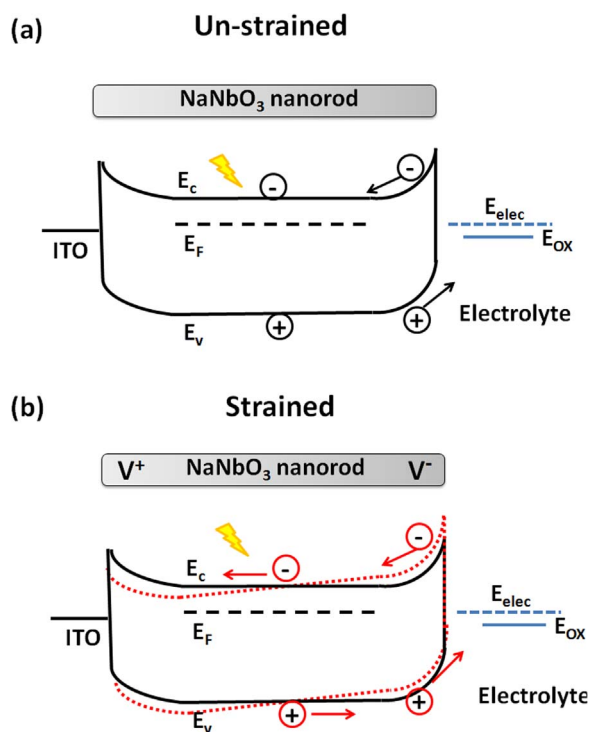


Fig. 6. Schematic representation of the PEC process. (a) Band structure of NaNbO_3 nanorods without piezopotential, (b) Band structure of NaNbO_3 nanorods with piezopotential.

lined stainless steel autoclave and kept into an oven at $150\text{ }^\circ\text{C}$ for 48 h for the hydrothermal treatment. After the hydrothermal reaction the resulting NaNbO_3 product was washed several times with deionized (DI) water and ethanol and dried at $70\text{ }^\circ\text{C}$ for 4 h.

4.2. Preparation of photoelectrodes

For photoelectrochemical activity tests, the photoelectrodes of NaNbO_3 nanostructures were prepared by depositing NaNbO_3 nanostructures onto flexible indium tin oxide (ITO) coated polyethylene terephthalate (PET) substrates using a spray coating method. Prior to deposition, a uniform suspension of NaNbO_3 nanostructures was prepared in 2-Propanol (2 mg/ml). In order to improve the adherence of the nanostructures with the substrate 2–3 drops of **Nafion binder** (全氟磺酸树脂粘合剂) were also added into the above suspension.

4.3. Characterization

X-ray diffraction measurements were carried out using a powder X-ray diffractometer (Rigaku Ultima-IV) with high intensity $\text{CuK}\alpha$ ($\lambda=1.54\text{ \AA}$) radiation source. Transmission electron microscopy (TEM) and high resolution transmission electron microscopy (HRTEM) images of the nanostructures were recorded on (JEOL, JEM-2200-FS) electron microscope operating at an accelerating voltage of 200 kV. X-ray photoelectron spectroscopy (XPS) measurements were carried out using SPECS system, equipped with a Mg ka (1253.6 eV) X-ray source. For the measurement, NaNbO_3 nanostructures were coated onto conducting indium tin oxide substrate. The base pressure in the instrument was kept $\sim 5 \times 10^{-11}$ Torr. It was operated in

fixed analyzer transmission mode with a pass energy of 40 eV. To remove the surface impurities a mild Ar ion sputter etching (~600 eV) was carried out for 30 s. The 30 s of Ar ion sputtering only reduces the surface impurities and do not removes the surface oxygen. In order to deal with potential charging issue, instrument uses electron flood gun operated at 270 V and 1.27 A. Also, the binding energy corrections were made using carbon peak (284.6 eV) as a reference. UV–visible spectrophotometer (Perkin Elmer, Lambda-1050) was used to determine the bandgap of the nanostructures. Piezoresponse force microscopy (PFM) measurements were performed on a commercial atomic force microscope instrument (Bruker, Dimension Icon) using Pt/Ir coated silicon probes.

4.4. Photocatalytic and piezophotocatalytic activity

For catalytic experiments, a 250 ml of (1×10^{-5} M) methylene blue (MB) organic dye solution containing 100 mg of photocatalyst (NaNbO_3) material was used. Catalytic experiments were performed in two different configurations i.e. (i) physical mixing, in which no ultrasonic vibrations were subjected to the catalytic system and (ii) with ultrasonic vibrations, where ultrasonic vibrator of power ~100 W and frequency ~40 kHz was used for generating piezopotential in the nanostructures. Before the start of each catalytic experiment, the MB dye solution containing NaNbO_3 nanostructures was vigorously stirred to establish adsorption–desorption equilibrium. Degradation capability of MB was evaluated under four conditions i.e. (i) under dark, (ii) dark with ultrasonic vibrations, (iii) under UV light irradiation and (iv) under both ultrasonic vibrations and UV light using the same material.

4.5. Photoelectrochemical and piezophotoelectrochemical activity

Photoelectrochemical measurements were performed in a standard three electrode assembly using a potentiostat (Biologic, SP-150). Photoelectrode comprising of NaNbO_3 nanostructure film coated onto flexible indium tin oxide (ITO) substrate was used as a working electrode. A platinum (Pt) wire and Ag/AgCl (3 M KCl) were used as counter and reference electrodes, respectively. For evaluating piezophotoelectrochemical activity, three electrode cell assembly was kept in an ultrasonic transducer (power ~100 W and frequency ~40 kHz) for generating piezopotential. A tungsten halogen lamp was used as a light source for the PEC measurements. A freshly prepared aqueous solution of Na_2SO_4 was used as an electrolyte for the measurements. The photocurrent measurements were performed at a scan rate of 10 mV/s. Electrochemical impedance spectroscopy (EIS) measurements was performed in the frequency range of 0.1 Hz to 1 kHz. Incident photon to current conversion efficiency (IPCE) was performed using a (Spe Quest) quantum efficiency measurement system.

Acknowledgements

The financial support from MeitY (Govt. of India) (RP02395) and DST-UKIERI (RP02893) projects are gratefully acknowledged. Authors

also acknowledge the XPS and HRTEM facilities at Physics department, IIT Delhi.

Appendix A. Supporting information

Supplementary data associated with this article can be found in the online version at doi:10.1016/j.nanoen.2017.05.029.

References

- [1] X. Wang, J. Zhou, J. Song, J. Liu, N. Xu, Z.L. Wang, *Nano Lett.* 6 (2006) 2768–2772.
- [2] Y. Hu, Y. Zhang, Y. Chang, R.L. Snyder, Z.L. Wang, *ACS Nano* 4 (2010) 4220–4224.
- [3] Q. Yang, W. Wang, S. Xu, Z.L. Wang, *Nano Lett.* 11 (2011) 4012–4017.
- [4] M. Peng, Y. Liu, A. Yu, Y. Zhang, C. Liu, J. Liu, W. Wu, K. Zhang, X. Shi, J. Kou, J. Zhai, Z.L. Wang, *ACS Nano* 10 (2016) 1572–1579.
- [5] Y. Su, Z. Wu, X. Wu, Y. Long, H. Zhang, G. Xie, X. Du, H. Tai, Y. Jiang, *Sens. Actuators A: Phys.* 241 (2016) 169–175.
- [6] F. Zhang, S. Niu, W. Guo, G. Zhu, Y. Liu, X. Zhang, Z.L. Wang, *ACS Nano* 7 (2013) 4537–4544.
- [7] Y. Zhang, Y. Yang, Z.L. Wang, *Energy Environ. Sci.* 5 (2012) 6850–6856.
- [8] X. Wen, W. Wu, Z.L. Wang, *Nano Energy* 2 (2013) 1093–1100.
- [9] Y. Liu, S. Niu, Q. Yang, B.D.B. Klein, Y.S. Zhou, Z.L. Wang, *Adv. Mater.* 26 (2014) 7209–7216.
- [10] C. Pan, M. Chen, R. Yu, Q. Yang, Y. Hu, Y. Zhang, Z.L. Wang, *Adv. Mater.* 28 (2016) 1535–1552.
- [11] H. Li, Y. Yu, M.B. Starr, Z. Li, X. Wang, *Phys. Chem. Lett.* 6 (2015) 3410–3416.
- [12] H. Li, Y. Sang, S. Chang, X. Huang, Y. Zhang, R. Yang, H. Jiang, H. Liu, Z.L. Wang, *Nano Lett.* 15 (2015) 2372–2379.
- [13] X. Li, J. Yu, J. Low, Y. Fang, J. Xiao, X. Chen, *J. Mater. Chem. A* 3 (2015) 2485–2534.
- [14] H. Wang, L. Zhang, Z. Chen, J. Hu, S. Li, Z. Wang, J. Liu, X. Wang, *Chem. Soc. Rev.* 43 (2014) 5234–5244.
- [15] Z.L. Wang, *Adv. Mater.* 24 (2012) 4632–4646.
- [16] J. Shi, M.B. Starr, H. Xiang, Y. Hara, M.A. Anderson, J.H. Seo, Z. Ma, X. Wang, *Nano Lett.* 11 (2011) 5587–5593.
- [17] X. Xue, W. Zang, P. Deng, Q. Wang, L. Xing, Y. Zhang, Z.L. Wang, *Nano Energy* 13 (2015) 414–422.
- [18] L. Yu, W. Chen, D. Li, J. Wang, Y. Shao, M. He, P. Wang, X. Zheng, *Appl. Catal. B Environ.* 164 (2015) 453–461.
- [19] S. Ji, H. Liu, Y. Sang, W. Liu, G. Yu, Y. Leng, *CrystEngComm* 16 (2014) 7598–7604.
- [20] T.Y. Ke, H.A. Chen, H.S. Sheu, J.W. Yeh, H.N. Lin, C.Y. Lee, H.T. Chiu, *J. Phys. Chem. C* 112 (2008) 8827–8831.
- [21] H. Shi, T. Wang, J. Chen, C. Zhu, J. Ye, Z. Zou, *Catal. Lett.* 141 (2011) 525–530.
- [22] S. Singh, N. Khare, *Chem. Phys. Lett.* 634 (2015) 140–145.
- [23] J. Lv, T. Kako, Z. Li, Z. Zou, J. Ye, *J. Phys. Chem. C* 114 (2010) 6157–6162.
- [24] Q. Gu, K. Zhu, N. Zhang, Q. Sun, P. Liu, J. Liu, J. Wang, Z. Li, *J. Phys. Chem. C* 119 (2015) 25956–25964.
- [25] P. Li, S. Ouyang, Y. Zhang, T. Kako, J. Ye, *J. Mater. Chem. A* 1 (2013) 1185–1191.
- [26] M.R. Gholipour, C.T. Dinh, F. Beland, T.O. Do, *Nanoscale* 7 (2015) 8187–8208.
- [27] R. Marschall, *Adv. Funct. Mater.* 24 (2014) 2421–2440.
- [28] M.H. Zhao, Z.L. Wang, S.X. Mao, *Nano Lett.* 4 (2004) 587–590.
- [29] H. Lee, J. Park, S.A. Han, D. Lee, K.B. Kim, N.S. Lee, J.Y. Park, Y. Seo, S.W. Lee, Y.J. Choi, *Scr. Mater.* 66 (2012) 101–104.
- [30] S. Singh, N. Khare, *RSC Adv.* 5 (2015) 96562–96572.
- [31] S. Khanchandani, S. Kumar, A.K. Ganguli, *ACS Sustain. Chem. Eng.* 4 (2016) 1487–1499.
- [32] Q. Liu, Y. Zhou, L. You, J. Wang, M. Shen, L. Fang, *Appl. Phys. Lett.* 108 (2016) 022902.
- [33] A.L. Sangle, S. Singh, J. Jian, S.R. Bajpe, H. Wang, N. Khare, J.L.M. Driscoll, *Nano Lett.* 16 (2016) 7338–7345.
- [34] Q. Li, M. Zheng, B. Zhang, C. Zhu, F. Wang, J. Song, M. Zhong, L. Ma, W. Shen, *Nanotechnology* 27 (2016) 075704.